High pressure ionic and molecular crystals of ammonia monohydrate within density functional theory

Gareth I.G. Griffiths, Alston J. Misquitta, A. Dominic Fortes, Chris J. Pickard, and Richard J. Needs

Citation: J. Chem. Phys. **137**, 064506 (2012); doi: 10.1063/1.4737887
View online: http://dx.doi.org/10.1063/1.4737887
View Table of Contents: http://jcp.aip.org/resource/1/JCPSA6/v137/i6
Published by the American Institute of Physics.

High pressure ionic and molecular crystals of ammonia monohydrate within density functional theory

Gareth I.G. Griffiths,[1] Alston J. Misquitta,[1] A. Dominic Fortes,[2] Chris J. Pickard,[3] and Richard J. Needs[1]
[1]*Theory of Condensed Matter Group, Cavendish Laboratory, J J Thomson Avenue, Cambridge CB3 0HE, United Kingdom*
[2]*Centre for Planetary Sciences at UCL/Birkbeck, University College London, Gower Street, London WC1E 6BT, United Kingdom*
[3]*Department of Physics and Astronomy, University College London, Gower Street, London WC1E 6BT, United Kingdom*

(Received 17 November 2011; accepted 5 July 2012; published online 13 August 2012)

A combination of first-principles density functional theory calculations and a search over structures is used to predict the stability of a proton-transfer modification of ammonia monohydrate with space group *P*4/*nmm*. The phase diagram is calculated with the Perdew-Burke-Ernzerhof (PBE) density functional, and the effects of a semi-empirical dispersion correction, zero point motion, and finite temperature are investigated. Comparison with MP2 and coupled cluster calculations shows that the PBE functional over-stabilizes proton transfer phases because too much electronic charge moves with the proton. This over-binding is partially corrected by using the PBE0 hybrid exchange-correlation functional, which increases the enthalpy of *P*4/*nmm* by about 0.6 eV per formula unit relative to phase I of ammonia monohydrate and shifts the transition to the proton transfer phase from the PBE pressure of 2.8 GPa to about 10 GPa. This is consistent with experiment as proton transfer phases have not been observed at pressures up to ∼9 GPa, while higher pressures have not yet been explored experimentally. © *2012 American Institute of Physics*. [http://dx.doi.org/10.1063/1.4737887]

I. INTRODUCTION

Ammonia monohydrate (AMH, $NH_3 \cdot H_2O$) exists as at least six different crystalline polymorphs over the experimentally studied range of pressures and temperatures of $0 < p < 9$ GPa and $170 < T < 295$ K.[1] Until recently the crystal structures of only two of these polymorphs had been determined: the low pressure phase AMH-I,[2,3] and the high pressure disordered body-centred-cubic phase AMH-VI.[4] Subsequently, a combination of *ab initio* random structure searching (AIRSS) (Refs. 5 and 6) and neutron powder diffraction led to the solution of the crystal structure of AMH-II,[7,8] and that of the related high-pressure ammonia dihydrate polymorph, ADH-II.[9] The structures of AMH-III and IV remain to be determined. Recently, Wilson *et al.* determined that the powder diffraction pattern identified as being due to a phase called AMH-V represents instead a mixture of high-pressure ammonia *hemi*hydrate, AHH-II, and ice VII.[10] The crystal structures and properties of ammonia hydrate polymorphs are of interest to planetary scientists due to the likely presence of substantial fractions of ammonia in ice accreted into the satellites of the gas giant planets.[11,12] While the relatively low abundance of ammonia relative to water in outer solar system ices leads planetary scientists to believe that ammonia dihydrate will be an important "rock-forming" mineral, the experimental data suggest the increased relevance of more ammonia-rich hydrates at elevated pressures. For example, ADH-II is known to break down to AMH-II + ice II upon warming, even at the modest pressures of 500 MPa, comparable to depths of just a few hundred kilometres inside the largest icy planetary bodies, Titan, Ganymede, and Callisto.[13,14] At pressures of 3–4 GPa, ADH-IV is also known to decompose to a lower hydrate + ice[13]: the recent work of Wilson *et al.*[10] has shown that this hydrate is in fact the same high-pressure hemihydrate produced by dissociation of AMH-IV. Hence, under pressure, there is the possibility for even water-rich liquids to crystallise – and thus fractionate – a very ammonia-rich crystalline phase. Such a pressure is relevant to the core of the large icy satellite Titan if it is undifferentiated (of uniform composition),[15] as well as during its initial accretion.[16] Such a pressure may also occur in the icy mantles of fully differentiated giant icy exoplanets or exomoons.[17] NH_3, H_2O, and CH_4 are likely to comprise a substantial fraction of the interiors of Uranus and Neptune at pressures up to 600 GPa and temperatures up to 7000 K.[18] The properties of this high *p*-*T* mixture are thought to be important in the generation of unusual magnetic fields in these bodies.[19]

The presence of weak hydrogen bonds and the occurrence of both homo- and hetero-nuclear hydrogen bonds in the ammonia hydrates provide a challenge for electronic structure methods, particularly with respect to the accuracy of exchange-correlation functionals in density functional theory (DFT) calculations. Standard functionals such as the Perdew-Burke-Ernzerhof (PBE) (Ref. 20) generalized gradient approximation (GGA) predict hydrogen-bonded molecular phases of AMH at low pressures, in agreement with experiment. We show here, however, that this approach predicts molecular AMH phases to be unstable with respect to the formation of ionic ammonium hydroxide (NH_4^+:OH^-)

proton-transfer phases at pressures of about 2.8 GPa, although no experimental evidence for such phases has been found to date. Including the weak dispersion forces, which are not described by standard density functionals such as the PBE-GGA, has a significant effect on the volumes and relative enthalpies of the phases in this system. The zero-point (ZP) motion of the H atoms is also important for an accurate account of the energetics. We have, moreover, found that the most serious defect of PBE calculations in this system is that the energetics of the proton transfer is very poorly described as too much electronic charge is transferred with the proton. We show that a satisfactory description of the experimental data, including the absence of proton-transfer phases at low pressures, requires the inclusion of nuclear ZP motion and accurate descriptions, beyond those afforded by functionals such as PBE-GGA, of both exchange interactions and the van der Waals forces that arise from electron correlation.

An important aspect of this work is the combination of first-principles DFT calculations with a random search strategy in order to identify new candidate high-pressure AMH structures. It was through the energetic ranking of the structures that deficiencies with the PBE functional were brought to light. Earlier DFT studies of ADH, AMH, AHH, and solid ammonia have revealed a propensity towards proton transfer at high pressures. Calculations have suggested that AMH-I transforms to ammonium hydroxide at ∼5 GPa,[21] AHH transforms to ammonium hydroxide ammoniate at ∼12 GPa,[22] and solid ammonia transforms to ammonium amide at ∼90 GPa.[23] The ionic solids derived from the two hydrates are isosymmetric with their molecular precursors, but there is no reason to suppose that other ionic structures might not be energetically stable. The non-trivial indexing and solution of a structure from neutron powder diffraction data at high pressure, and the tendency towards the formation and/or persistence of metastable phases in low-temperature condensed molecular systems on laboratory timescales motivates the computational prediction of equilibrium crystal structures and their physical properties.

In Sec. II, we present results using the PBE functional, including a random-structure search that revealed a new ionic crystal structure. We calculate the thermodynamic stability of the new ionic phase and all other known molecular and ionic AMH crystals with respect to one another, and in Sec. III we examine the consequences of adding zero-point motion and finite temperature effects for these computed stabilities. Section IV further considers the inclusion of a dispersion correction, and in Sec. V we compare the effect of these differing computational techniques on the calculated bandgaps of the molecular and ionic phases. Finally, we discuss the possible relevance of the newly identified ionic phase to experimental studies of the high-pressure phase diagram of AMH.

II. RESULTS WITH THE PBE AND RELATED FUNCTIONALS

With the aim of accurately determining the thermodynamic stabilities of the various crystalline phases reported here, we began by performing static calculations using the PBE functional, both with and without the G06 semi-empirical dispersion correction,[24] before subsequently considering the more computationally demanding effects of ZP motion and exact exchange.

The CASTEP plane wave code[25] was used for all of the calculations on periodic crystals. We used ultrasoft pseudopotentials[26] for the PBE and PBE+G06 calculations, and norm-conserving pseudopotentials generated with the OPIUM software[27] for calculations using the PBE0 hybrid functional, which includes 25% Hartree-Fock exchange.[28] All of the results reported in this paper with the ultrasoft pseudopotentials were obtained by refining the structures to a high level of accuracy consisting of a plane wave cutoff energy of 700 eV and a Monkhorst-Pack (Ref. 29) Brillouin zone sampling grid of spacing $2\pi \times 0.04$ Å^{-1}. The enthalpy difference between AMH-I and the ionic *P*4/*nmm* phase of AMH reported here was changed by less than 0.0002 eV per AMH formula unit (f.u.) on doubling the cut off energy to 1400 eV, while the enthalpy change on doubling the number of k-points was even smaller. Forces were converged to better than 0.005 eV/Å, while the stress on the unit cell was converged to better than 0.01 eV/Å^3. The norm-conserving pseudopotentials required a plane wave cutoff energy of 1000 eV, for which the energy difference between AMH-I and *P*4/*nmm* was converged to better than 0.00002 eV per f.u. A less dense Brillouin zone sampling grid spacing of $2\pi \times 0.05$ Å^{-1} was used for the PBE0 calculations, which gave an energy convergence of better than 0.03 eV per f.u.

We initially considered the stability of the molecular polymorphs AMH-I ($P2_12_12_1$) and AMH-II (*Pbca*); in the latter case we computed the stability of forms with two subtly different H-bonding schemes as found by neutron diffraction and from *ab initio* structure searches. We also calculated the stability of the ionic ammonium hydroxide crystal, which is isosymmetric with AMH-I (i.e., space-group $P2_12_12_1$), obtained by proton transfer in DFT calculations by Fortes *et al.*[21] The PBE and PBE+G06 enthalpies of these candidate phases, relative to that of AMH-II, are shown in Figs. 1(a) and 1(b), and the transition pressures are summarised in Table I. These reveal that the calculated pressures of the AMH-I to AMH-II transition are substantially over-estimated, being ∼3 GPa with PBE, reducing to 1 GPa with PBE+G06, compared with the experimentally observed value of around 0.4 GPa.[8] It is interesting to note the difference in enthalpy of around 0.01 eV per f.u. (giving an increase in transition pressures of around 1 GPa) between the two subtly different H-bonded forms of AMH-II. The ionic $P2_12_12_1$ structure becomes more energetically favourable than AMH-I above 4.5 GPa (agreeing well with the value of 5 GPa found in the earlier work),[21] and more favourable than AMH-II above 6 GPa. Although the ionic $P2_12_12_1$ phase has a region of thermodynamic stability on this phase diagram relative to the known molecular phases, there is good reason to believe that it is not the most stable phase of AMH at high pressure. Experimentally, AMH-II is observed to transform to AMH-III on warming above 210 K at 1 GPa, and to AMH-IV on compression above 2.2 GPa on the 170 K isotherm.[1] Although the structures of these two phases are unknown, it is clear that neither of them are the ionic $P2_12_12_1$ phase.[21] We were therefore motivated to discover whether

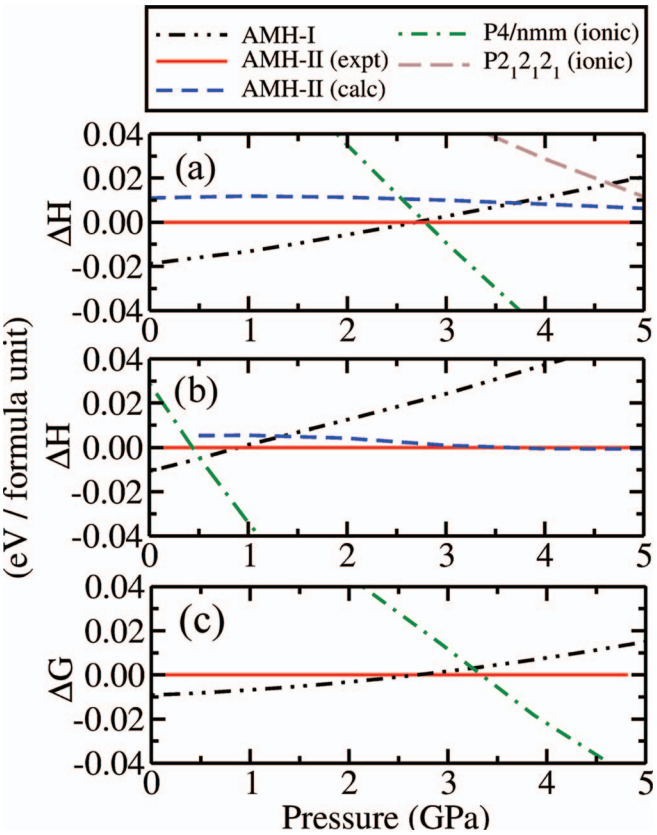

FIG. 1. Enthalpies per f.u. of AMH structures relative to AMH-II calculated with: (a) the PBE functional, (b) the PBE functional and G06 semi-empirical dispersion correction. The Gibbs free energy per f.u. of AMH structures relative to that of AMH-II is shown in (c), calculated with the PBE functional including vibrational motion at 175 K. AMH-II (expt) denotes the experimental structure, while AMH-II (calc) denotes the structure found in the AIRSS study reported in Ref. 7. Note that the AMH-II structure was not studied with PBE0 because of its large size.

any other, hitherto unknown, structures could be identified using our well-established AIRSS method.[5,6] As described in Sec. II A, this work predicted the occurrence of a new ionic structure in space-group *P*4/*nmm*.

A. *Ab initio* Random structure searching

We have employed the AIRSS method to relax a total of around 7700 trial structures, encompassing searches in unit cells containing 2, 3, 4, 5, 6, and 8 f.u. of AMH. The PBE functional was used for the AIRSS relaxations, as PBE+G06 gives arguably worse energetics than the already over-bound PBE, while PBE0 is orders of magnitude too computationally demanding, as discussed in Secs. II B and II C. Further details of the searching methodology are given in the supplementary material.[45]

In our previous work,[7] AIRSS was used with the PBE functional to determine the correct crystal structure of AMH-II using only the experimentally determined unit-cell volume and symmetry as initial constraint. This structure, with 112 atoms (16 f.u.) in the unit cell, was found to be in near perfect agreement with that obtained by a direct-space solution of the crystal structure from neutron powder diffraction data, differing only in the minute detail of the hydrogen-bonding.[7] It is likely that the exact experimental structure, with the alternate H-bond scheme, could have been found if more searches had been performed. In this work, AIRSS found the low-pressure orthorhombic AMH-I phase several times, but did not reproduce the discovery of AMH-II as searching was performed in variable unit cells containing a maximum of 8 f.u. Our searches did not find any molecular structures more stable than AMH-I and II. This indicates that if any of the remaining unsolved AMH phases are molecular they are likely to have complex structures with more than 8 f.u. per unit-cell. It would be possible to search for such structures in larger unit cells than are currently practical with DFT using an interaction potential constructed by fitting to coupled-cluster single double triple (CCSD(T)) (or similar) results. Such an interaction potential would have to carefully account for polarization effects and the flexibility of the molecules and ions over a pressure range of 10 GPa in which the volume decreases by about 45%.

Further searching with AIRSS revealed an entirely new structure (shown in Fig. 2) with space group *P*4/*nmm* to be the most thermodynamically stable in all 2 f.u. searches at 10 GPa. Subsequent searches with 4 f.u. at both 3 and 10 GPa also showed *P*4/*nmm* to be the most stable structure regardless of the constraints imposed. Ultimately, even the searches with 8 f.u. found the *P*4/*nmm* structure to be the most stable. None of the searches performed with 3, 5, or 6 f.u. yielded structures with enthalpies as low as that of *P*4/*nmm*, which was found a total of 42 times in the AIRSS calculations. Importantly, the *P*4/*nmm* structure was found both in searches that were completely unconstrained, and those with the

TABLE I. Summary of the transition pressures between AMH phases with several methods.

	Transition pressure (GPa)		
Method	AMH-I → AMH-II	AMH-II → *P*4/*nmm*	AMH-I → *P*4/*nmm*
PBE	2.7	2.8	2.8[a]
PBE+G06	0.9[a]	0.4[a]	0.5
PBE+ZP (175 K)	2.7	3.3	3.3[a]
PBE0	n/a	n/a	10.8
PBE0+ZP+G06 (0 K)	n/a	n/a	8.8
Experiment (180 K) (Ref. 7)	0.5	n/a	n/a

Note: PBE0 calculations were not performed for the AMH-II phase and are, therefore, not included in the table (n/a).
[a]Transitions that would occur at a pressure at which neither phase is thermodynamically stable.

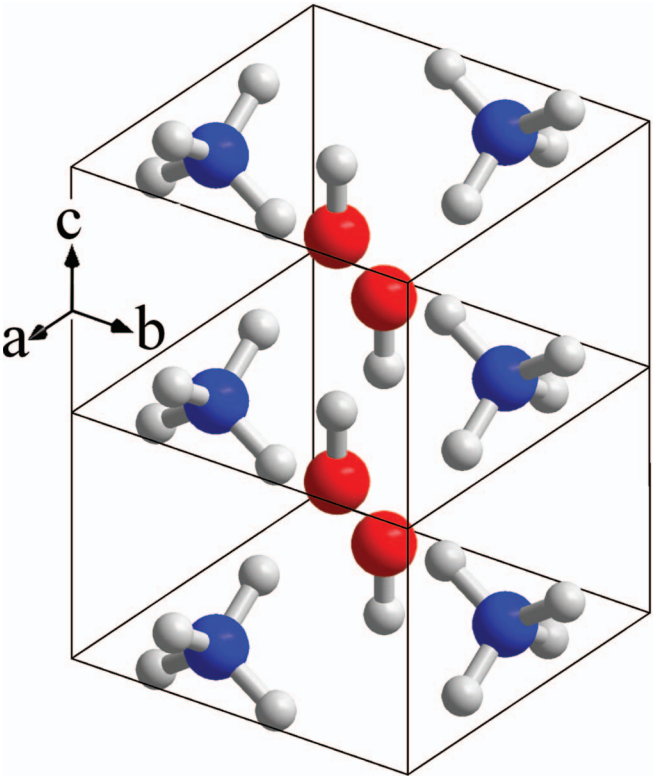

FIG. 2. The *P4/nmm* ionic structure; light grey atoms are hydrogen, red atoms are oxygen, and blue atoms are nitrogen. The solid lines depict two unit-cells, the orientation of the crystallographic axes being indicated on the left.

constraints described in the supplementary material.[45] This provides evidence that, regardless of the constraints, the energy landscape has been well sampled up to 8 f.u.

The relative enthalpy of the ionic *P4/nmm* structure, computed with the PBE functional, is shown in Fig. 1(a). We find that its enthalpy declines very rapidly with pressure, such that it allows AMH-II only the narrowest window of thermodynamic stability (∼0.01 GPa) with the PBE functional, and no region of stability at all with PBE+G06. This result is difficult to reconcile with the existing experimental results, which clearly demonstrate a wide region (at least 2 GPa) over which AMH-II is stable.

We proceed by making a more detailed analysis of these static PBE based results, studying the effects of explicitly including non-local exchange interactions with the PBE0 functional, and then moving on to evaluate the effects of zero-point motion, temperature, and dispersion forces.

B. Calculations for molecular and ionic fragments

To obtain insight into the problem highlighted above we have selected fragments of the AMH-I and *P4/nmm* crystals (at pressures of 1 and 4 GPa, respectively) for a more detailed analysis. These fragments were chosen to be representative of the interactions in the crystal and consisted of pairs of molecules/ions in close proximity: NH_3 and H_2O for the AHM-I crystal (Fig. 3) and NH_4^+ and OH^- ions for the *P4/nmm* crystal (Fig. 4). In Figs. 3 and 4, we plot interaction energies for these pairs calculated using the supermolecular

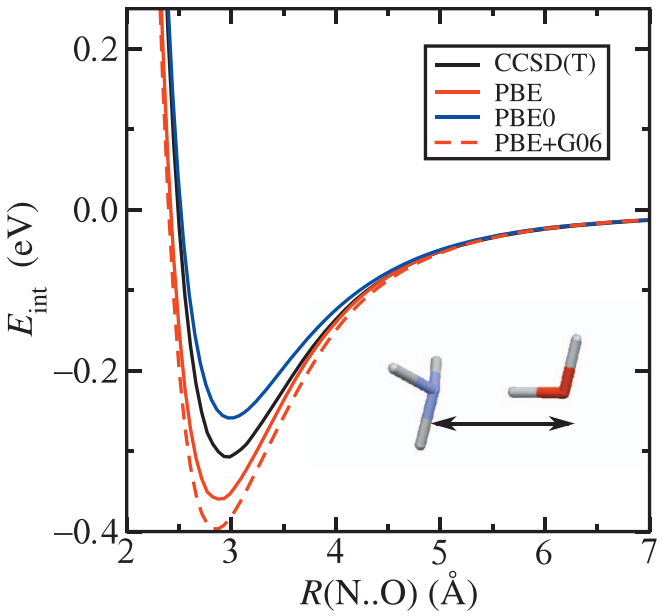

FIG. 3. Interaction energy against separation of NH_3 and H_2O for a configuration taken from the AMH-I molecular phase.

approach, that is, $E_{int} = E(AB) - E(A) - E(B)$, where $E(A)$ and $E(B)$ are the energies of the monomers, and $E(AB)$ is the energy of the complex. We have used CCSD(T) and MP2 as reference methods, although the MP2 results are not shown as they are essentially identical to those from CCSD(T). The CCSD(T) results are compared with PBE, PBE+G06, and PBE0 density functional results.

We have calculated counterpoise-corrected interaction energies using the Boys and Bernardi[30] scheme with a Sadlej-pVTZ basis[31] augmented with a small set of "bond centered functions"[32] which help to saturate the dispersion energy.[33]

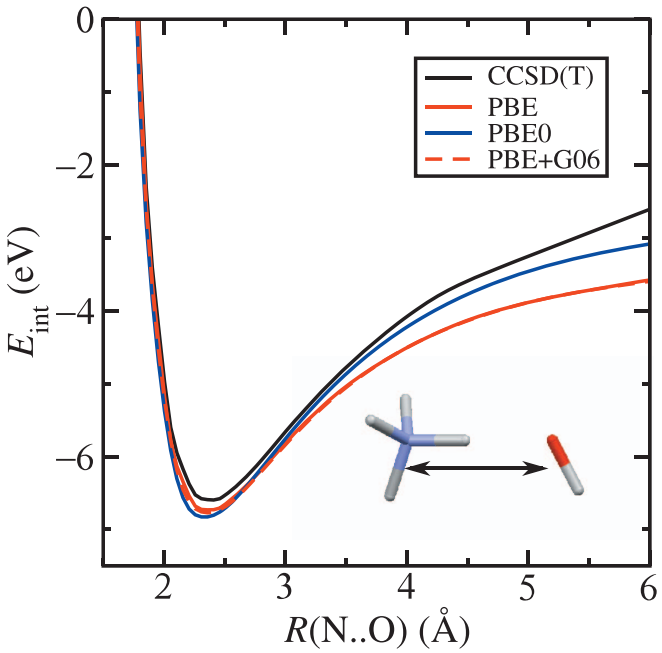

FIG. 4. Interaction energy against separation of NH_4^+ and OH^- for a configuration taken from the *P4/nmm* ionic phase.

TABLE II. The bulk modulus (K), the first pressure derivative of the bulk modulus (K'), and the equilibrium volume (V_0). Fitting ranges: AMH-I 0–2.5 GPa, AMH-II 0.4–2.5 GPa. *P*4/*nmm* PBE 3–6 GPa, PBE+G06 0–2.5 GPa.

Structure	Method	K (GPa)	K'	V_0 (Å^3)
AMH-I ($Z = 4$)	PBE	9.7	5.0	245.04
	PBE+ZP (0 K)	12.5	2.4	241.50
	PBE+ZP (175 K)	12.2	2.4	242.17
	PBE+G06	12.5	6.3	218.10
	Experiment (140 K) (Ref. 1)	8.9(4)	4.2(3)	247.66
	Experiment (180 K) (Ref. 7)	7.33(3)	5.3	248.00(2)
AMH-II ($Z = 16$)	PBE	8.1	5.5	971.60
	PBE+ZP (0 K)	9.6	3.1	973.22
	PBE+ZP (175 K)	9.2	3.0	983.25
	PBE+G06	13.4	4.2	842.70
	Experiment (180 K)	7.2(3)	5.3(2)	947(2)
*P*4/*nmm* ($Z = 2$)	PBE	3.8	13.8	106.51
	PBE+ZP (0 K)	4.6	7.4	113.13
	PBE+ZP (175 K)	4.5	5.4	117.95
	PBE+G06	20.8	11.0	83.01

Selected calculations with the larger aug-cc-pVTZ basis set suggest that the CCSD(T) interaction energies are converged to within 5% at the equilibrium geometry and better at larger separations. These calculations were performed using the DALTON 2.0 program.[34] For a deeper insight into the interaction energies we have additionally used the CAMCASP program[35] to perform symmetry adapted perturbation theory (SAPT (DFT)) (Refs. 36–38) calculations to decompose the interaction energies into physical components.

Figure 3 shows that PBE overbinds the $NH_3\cdots H_2O$ complex, although the equilibrium bond length agrees reasonably well with the CCSD(T) value. The overestimation of the bulk modulus (K) of AMH-I reported in Table II may be a reflection of the overbinding of PBE and the consequent overestimate of the curvature of the potential well. In contrast, PBE0 underbinds the complex, but results in an equilibrium separation in near perfect agreement with the CCSD(T) calculations. The SAPT(DFT) energy decomposition shows that asymptotically the $NH_3\cdots H_2O$ interaction is dominated by the dipole-dipole electrostatic energies with the dispersion and polarization energies being negligible. Consequently, it is not a surprise that both the correlated and density-functional methods agree in this region.

The ionic system behaves very differently from the molecular one. Note that the interaction energies for the ionic system shown in Fig. 4 are an order of magnitude larger than in the molecular system. The SAPT(DFT) results show that the energetics are almost completely dominated by the charge-charge electrostatic interaction between the ions, with the dispersion energy contribution being insignificant even at the relatively short N···O separation of 2.5 Å. This is exactly the kind of system for which local and semi-local density functionals are expected to achieve high accuracy. Indeed, the PBE and PBE0 energies are close to the CCSD(T) result at the equilibrium geometry and on the repulsive wall. In contrast to the molecular system, however, PBE significantly overbinds the ionic complex at large separations. As can be seen in Fig. 4, the overbinding compared with CCSD(T) is 20% at 5 Å but it grows to more than 50% at 6.5 Å. The interaction energies are still relatively large at these separations, and consequently these errors have important effects within the crystal. This is consistent with our observation that the *P*4/*nmm* ionic phase is over-stabilized with respect to the molecular phases.

A partial charge analysis shows that the substantial difference between the PBE and CCSD(T) interaction energies at large separations is a consequence of excessive charge transfer. Within PBE the magnitude of the charges on the monomers grows as they are pulled apart, becoming as large as $\pm 1.2e$ at a N···O separation of 6.5 Å. In contrast, the CCSD(T) potential energy curve can be fitted very well with a $-1/R$ form corresponding to partial charges of $\pm 1e$. The PBE charge transfer error is analogous to the delocalization or static correlation errors exhibited by local and semi-local density functionals.[39] This error can be at least partially corrected by introducing some fraction of non-local exchange. Using PBE0 gives a significant improvement upon the PBE energies, with the overbinding compared with CCSD(T) at 5 Å and 6.5 Å reduced to 6% and 28%, respectively, see Fig. 4.

C. PBE0 calculations for crystalline AMH

As the PBE0 functional offers a partial solution to the charge transfer errors which arise with PBE, we performed calculations for the molecular AMH-I and ionic *P*4/*nmm* phases using the PBE0 hybrid functional. Because of the slow convergence of the exchange terms with distance, the PBE0 calculations for the crystal were as much as two orders of magnitude more computationally expensive than the corresponding PBE calculations. For this reason, geometry optimizations were not possible with PBE0 and instead we performed single-point energy calculations using the relaxed PBE structures. We attempted to obtain equation of state parameters from the PBE0 results for AMH-I and

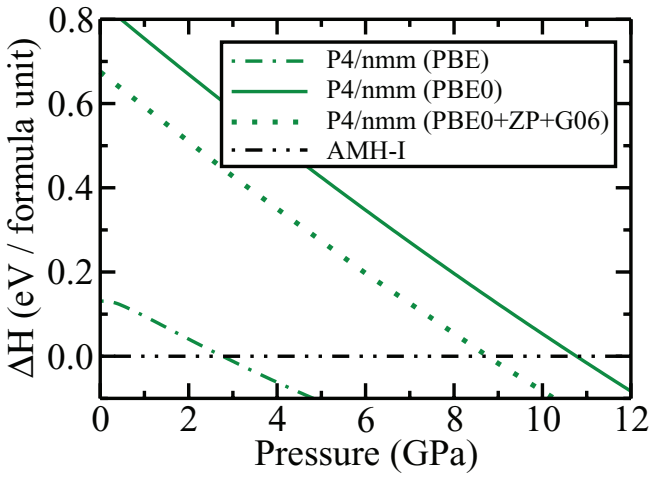

FIG. 5. Enthalpies per f.u. of *P*4/*nmm* relative to AMH-I from three methods; the PBE functional, the PBE0 hybrid functional, and PBE0 with both the G06 dispersion correction and ZP vibrational motion effects included. The PBE0 calculations were performed on the structures relaxed with the PBE functional.

*P*4/*nmm*. The calculated energies were fitted to the third-order Birch-Murnaghan equation of state and the pressure was obtained by differentiation. We obtained equilibrium volumes of $V_0 = 220$ Å^3 for AMH-I and $V_0 = 172$ Å^3 for *P*4/*nmm*, which are similar to those obtained from the PBE+G06 calculations. We were not able to obtain reliable estimates of K or K' from our PBE0 data as the values were sensitive to the data and fitting procedure. The use of the PBE structures for the PBE0 calculations is an approximation. However, we believe this approach to be reasonably robust because enthalpies obtained using partially relaxed PBE structures were almost identical to those from the fully relaxed structures.

Mulliken charge analysis of the *P*4/*nmm* crystal suggests that the electronic charge transfer between the "OH^-" and "NH_4^+" ions is about 0.70*e* when using the PBE functional and 0.55*e* with PBE0. The improved description of the ionic phase provided by PBE0 destabilizes the *P*4/*nmm* ionic phase relative to AMH-I, and consequently *P*4/*nmm* enters above 10.8 GPa, as can be seen in Fig. 5. AMH-II, AMH-IV, and AMH-VI are not present on this phase diagram, but they are expected to have regions of stability between AMH-I and *P*4/*nmm*, pushing the entry of the new ionic phase to even higher pressures.

III. ZERO-POINT MOTION AND FINITE TEMPERATURE EFFECTS

The relatively small mass of hydrogen leads to large ZP motions in AMH, where 5 out of 7 nuclei are protons. The ZP motion in AMH may lead to important differences in the relative stabilities of the phases, particularly when comparing a dense ionic phase with a less dense molecular one. We have investigated the effects of ZP motion on the phase diagram of AMH within the quasi-harmonic approximation with the supercell method and finite atomic displacements. The quasi-harmonic approximation normally gives a reasonable description of vibrational effects, including thermal expansion.

We calculated the phonons of AMH-I and *P*4/*nmm* in 112 atom supercells, while a set of finite displacement phonon calculations were performed for AMH-II, which has a 112 atom primitive cell. Care was taken to ensure that the structures were very well relaxed prior to performing phonon calculations, ensuring that any stresses on the unit cell were less than 0.01 eV/Å^3 and that the forces were converged to within 0.005 eV/Å (0.003 eV/Å for AMH-II). In addition, the fine grid on which the augmentation charge density for the ultrasoft pseudopotentials is represented was increased to 2.75 times the multiple of the wavefunction grid to obtain higher accuracy.

The Gibbs free energy at 175 K is plotted against pressure for AMH-I, AMH-II, and the *P*4/*nmm* ionic phase in Fig. 1, as calculated with the PBE functional. The phonon pressure was evaluated from the derivative of the ZP energy (or Helmholtz free energy at finite temperature) with respect to volume. The total pressure is the sum of the static DFT and phonon pressures. The larger density of the ionic *P*4/*nmm* phase leads to higher phonon frequencies and hence destabilization relative to the molecular phases. The pressure obtained within PBE at which *P*4/*nmm* becomes the most stable at 175 K is increased by 0.55 GPa–3.32 GPa. The inclusion of vibrational effects increases the pressure interval of stability of AMH-II to about 0.7 GPa, although this is still smaller than the experimental interval of about 1.7 GPa.[1,7]

The inclusion of vibrational effects on top of PBE0 further destabilizes *P*4/*nmm* and it only becomes stable above 11.3 GPa, although conversely the inclusion of the G06 dispersion correction reduces the transition pressure to 8.8 GPa, as shown in Fig. 5.

Experimentally, the transition from AMH-I to AMH-II at ~0.35 GPa results in a volume decrease of 4.6%.[8] Both PBE, and PBE with ZP motion at 175 K, give only a 2% decrease in volume at this transition, whereas PBE with the G06 dispersion correction gives a decrease of 3.4%.

Data from fits of the calculated pressure-volume data to the third-order Birch-Murnaghan equation of state,[40] with and without the ZP motion and temperature contributions, are shown in Table II. The uncorrected PBE results compare favorably with the experimental equilibrium volume, bulk modulus, and the first pressure derivative of the bulk modulus for both AMH-I and AMH-II. It is interesting to note that there is one exception to the expected increase in volume from including ZP motion, AMH-I is seen to shrink slightly when ZP motion is taken into account. All three structures are found to increase in volume when thermal effects are included at 175 K, accompanied by a small reduction in the bulk moduli relative to the values obtained on including ZP motion at 0 K.

IV. DISPERSION CORRECTION

The computed phase stabilities change substantially with the inclusion of the G06 correction to the PBE functional, as shown in Fig. 1(b). Additionally, each phase undergoes a large contraction of the volume when the G06 correction is included.

The large effect of the dispersion correction on the ionic structure may seem paradoxical as it amounts to a relatively small fraction of the binding energy of the $NH_4^+ \cdots OH^-$ ionic

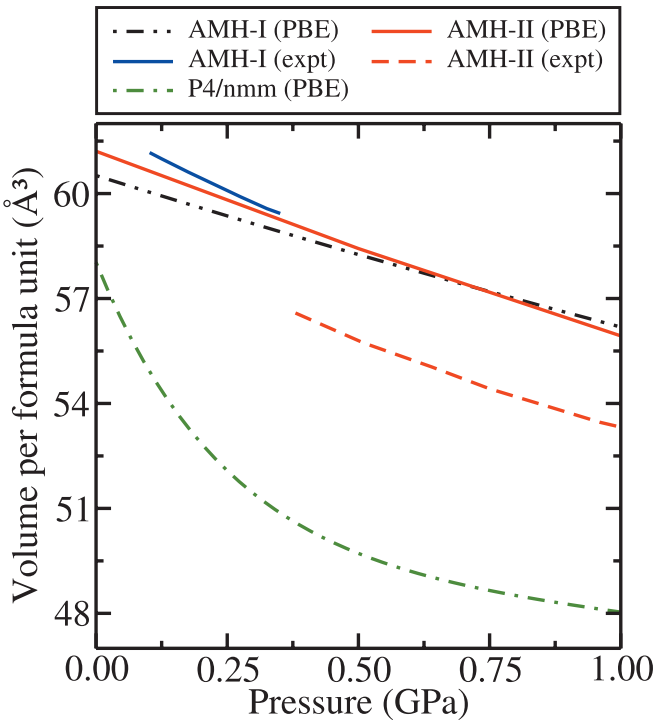

FIG. 6. Volume-pressure relationships for the AMH-I and AMH-II phases and the new ionic phase of AMH reported here, calculated with the PBE functional, including the effects of ZP motion and temperature (175 K). The experimental data were obtained from deuterated samples at 180 K at the Institut Laue Langevin, in the gas pressure cell with a high-resolution powder diffractometer, and from a Paris-Edinburgh cell study with a high-intensity powder diffractometer, for AMH-I and AMH-II, respectively.[8,42]

complex (see Fig. 4). The rapid reduction in the volume of *P*4/*nmm* with applied pressure apparent in Fig. 6 is almost entirely associated with a contraction along the **c** direction. As shown in Fig. 9, the hydrogen bonds form a square net within the **a**-**b**-planes of *P*4/*nmm*, but there is no apparent hydrogen bonding between the layers, and therefore it is very soft in the **c** direction, as demonstrated in Fig. 7.

V. BANDGAPS OF THE PHASES

The minimum bandgaps obtained with the PBE and PBE0 functionals are shown in Fig. 8 calculated using the

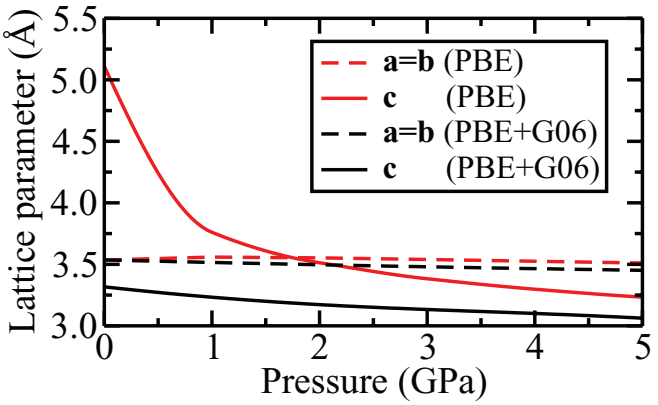

FIG. 7. Variation of the lattice parameters with pressure for the *P*4/*nmm* ionic phase, calculated with the PBE functional, with and without the G06 dispersion correction.

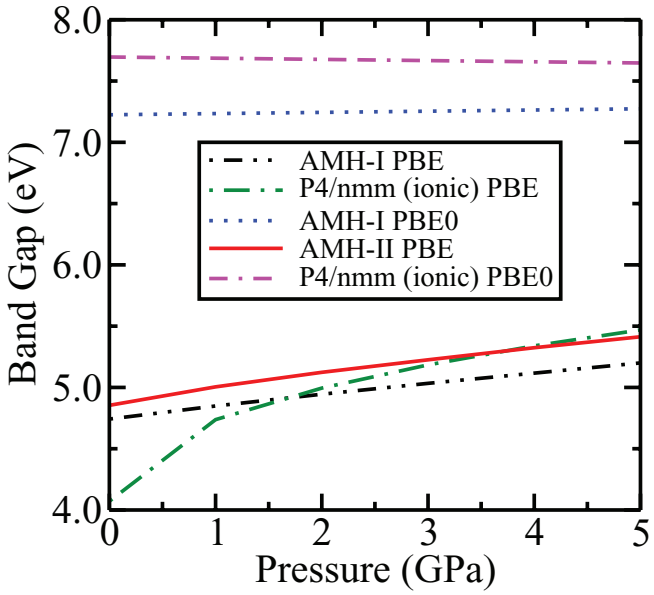

FIG. 8. Variation of the bandgaps of the phases with pressure. AMH-I (and AMH-II using PBE only) have direct bandgaps, while both the PBE and PBE0 calculations predict that the *P*4/*nmm* phase has an indirect bandgap. The PBE0 calculations were performed using the PBE structures.

LINDOS code.[41] While the molecular structures have direct bandgaps, both PBE and PBE0 calculations predict *P*4/*nmm* to have an indirect bandgap. The bandgaps provided by the PBE0 functional, which includes explicit exchange interactions, are substantially larger than those predicted by PBE.

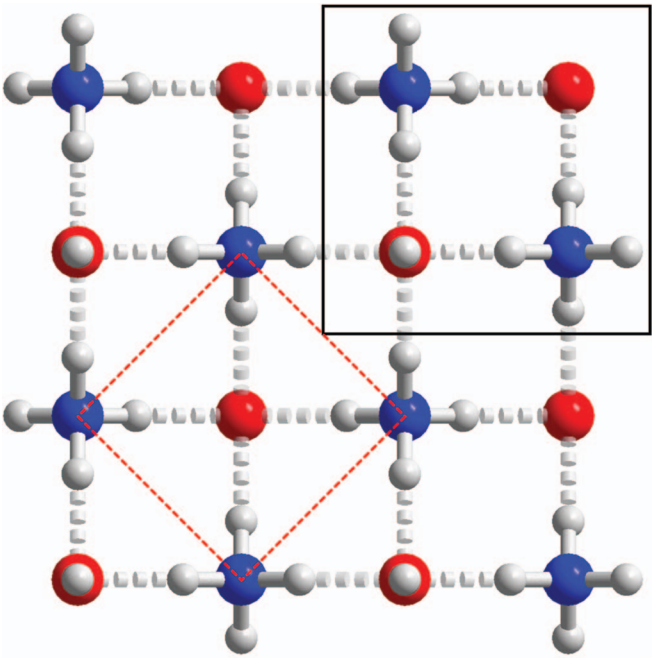

FIG. 9. The ionic *P*4/*nmm* phase viewed along the **c**-axis. This structure comprises sheets of ions hydrogen-bonded together (dashed rods) donated by the ammonium ions to the hydroxide. The hydrogen atom of the hydroxide ion points directly along the **c**-axis and does not appear to participate in a hydrogen bond. Hence, the layers are not H-bonded to one another and consequently the structure exhibits a large compressibility along the **c**-axis. The dashed line shows the basis of a cubic structure that may be derived from the tetragonal cell (marked by the solid black line) by a small distortion, as discussed in the text.

TABLE III. Structure of the *P*4/*nmm* ionic phase at 3 GPa with the PBE functional (primitive cell, $Z = 2$).

Functional	Lattice parameters (Å, °)			Atom	Site	Wyckoff symbol	Fractional atomic coordinates		
PBE	$a = 5.006$	$b = 5.006$	$c = 3.385$	N	−42	2a	0.25	0.7500	0.0000
	$\alpha = 90$	$\beta = 90$	$\gamma = 90$	O	4 *mm*	2c	0.25	0.2500	0.6562
				H1	4 *mm*	2c	0.75	0.7500	0.6308
				H2	.*m*.	8i	0.25	0.5727	0.8262

VI. THE *P*4/*nmm* STRUCTURE AND POSSIBLE RELATIONSHIP TO AMH-VI

Our PBE calculations predict that the ionic *P*4/*nmm* phase should be thermodynamically stable across a broad region of the high-pressure phase diagram. Whether *P*4/*nmm* corresponds to any of the polymorphs with as-yet undetermined structures (AMH-III or -IV), was not clear initially due to a lack of suitable experimental data. The published neutron powder diffraction data for AMH-III and -IV, either of which may be ionic, are not of high quality;[1,3] in particular, the published powder pattern of AMH-IV consists only of very broad peaks. We therefore carried out our own neutron powder diffraction study,[42] with the aim of obtaining higher resolution data from these polymorphs. The results acquired so far show that neither of these polymorphs is likely to be the *P*4/*nmm* phase, and indeed both appear likely to be extremely complex structures with > 8 f.u. per unit cell. Therefore, future *ab initio* searches in this larger region of parameter space will be necessary if the computational expense is not prohibitive.

However, a closer examination of the *P*4/*nmm* structure does reveal a discernible relationship to the known high-pressure body-centred-cubic (bcc) phase AMH-VI,[4] even though the calculated diffraction patterns differ considerably. Indeed these differences are readily attributed to the splitting of reflections caused by the distortion of the ionic phase from ideal cubic symmetry.

The bcc crystal AMH-VI was first produced by warming AMH-IV at 6.5 GPa above 280 K,[1] Its structure is reported to consist of orientationally and positionally disordered NH_3 and H_2O molecules.[4] Interestingly, a similar bcc phase of ADH was reported by Fortes *et al.*,[14] and subsequently confirmed by Loveday *et al.*,[43] and a bcc form of AHH has very recently been discovered by Ma *et al.* by compression of AHH-II above 19 GPa at room temperature.[44] It seems very likely that a bcc solid solution exists across a substantial portion of the water-ammonia binary phase diagram at high pressure, from ADH, through AMH to AHH. The occurrence of this solid solution may have significant implications for the formation and evolution of ammonia-bearing icy planetary bodies.

The hydrogen-bonded layers in the *P*4/*nmm* ionic phase (Fig. 9) form a network with a square motif, which defines the tetragonal unit cell (marked in black). However, an oblique cell (dashed line) is also marked that closely approximates a cube having ammonium ions at the corners and a hydroxide ion near the center. A slight shrinkage of the tetragonal **a**- and **b**-axes (∼4.4% relative to the value given in Table III) while keeping the length of the **c**-axis unchanged, forms a perfect cube. Furthermore, shifting the fractional z-coordinate of the oxygen atom from 0.6562 to 0.5 yields a heavy-atom structure of space-group $Pm\bar{3}m$, $\mathbf{a} = 3.3850$ Å, and fractional atomic coordinates N = 0, 0, 0, and O = 0.5, 0.5, 0.5. Finally, mixing the occupancies of these two sites with ammonium and hydroxyl ions gives an ionic equivalent of the AMH-VI structure.

Clearly, it is necessary to include the bcc AMH-VI structure in our calculation framework in order to construct a complete computational phase diagram. However, the disordered nature of AMH-VI precludes straightforward investigation using DFT but, as a first approximation, a so-called "shaking" search was performed, in which a $2\times2\times2$ supercell comprising only the oxygen and nitrogen atoms was created. For each search, the appropriate number of hydrogen atoms were distributed randomly over the supercell and the atomic positions were relaxed. The lowest enthalpy structure, which was obtained repeatedly, does not appear in Fig. 1 as it lies ∼0.2 eV per f.u. above AMH-II and is quite far from thermodynamic stability. The large discrepancy between the computed stability and the reproducible experimental observation of AMH-VI may be due to the small cell used in the calculations.

Given the highly disordered nature of AMH-VI, the differences in calculated Bragg intensities between the proposed molecular model and a possible ionic variant are small. It is our hypothesis that in fact the AMH-VI powder data may be equally well fitted by a disordered ionic structure as by a disordered molecular structure. Making a distinction between these two models will require future spectroscopic analyses. Given that we have obtained an ionic phase with a high degree of thermodynamic stability, which appears to be simply an ordered (and consequently slightly distorted) modification of AMH-VI, we suggest that this lends weight to the possibility that AMH-VI itself is also ionic.

VII. CONCLUSIONS

We have performed extensive *ab initio* searches for new phases of AMH at pressures up to 12 GPa using the PBE functional and found a new thermodynamically stable ionic structure of space group *P*4/*nmm*. The relationship described earlier between the structures of *P*4/*nmm* and AMH-VI may indicate that we have discovered an ordered ionic variant of AMH-VI. Alternatively, the *P*4/*nmm* phase may be related to one of the two experimentally observed AMH phases (III, IV) whose structures are unknown. As the *P*4/*nmm* phase was the only new structure predicted to be thermodynamically stable within some pressure range, it is likely that if it is one of the

two unknown AMH structures, then the other will have a unit cell with $Z > 8$.

With the PBE functional, we found that the *P*4/*nmm* phase became stable at 2.8 GPa, which is at odds with the available experimental data. Subsequent investigations into the effects of temperature, ZP motion, and dispersion forces found that the latter two play a substantial role in determining the relative stabilities of the phases. The inclusion of ZP motion destabilizes the dense *P*4/*nmm* ionic phase; conversely the dispersion correction leads to a significant underestimation of the transition pressure from molecular AMH to ionic *P*4/*nmm*.

Accurate CCSD(T) calculations on representative complexes from the ionic and molecular AMH phases revealed that the PBE functional substantially overbinds the ionic phase. We have presented evidence that this overbinding arises from an overestimate of the electronic charge transfer accompanying the proton transfer, which can be partially remedied by using the hybrid PBE0 functional. PBE0 calculations gave an increase in the enthalpy of the ionic *P*4/*nmm* phase by about 0.6 eV per f.u. relative to AMH-I. The transition pressure from AMH-I to *P*4/*nmm* phase is substantially increased, which eliminates the inconsistency with experiment. This failure of the PBE functional, for an electrostatic-bound system for which GGA-type density functionals are typically assumed to be accurate, is likely to have implications for other systems. Further experimental work is necessary to explore the phase diagram of AMH at 9 GPa and above to confirm our assignment of *P*4/*nmm* as a stable ionic phase of AMH.

ACKNOWLEDGMENTS

This work was supported by the Engineering and Physical Research Council (EPSRC) of the UK. Computational resources were provided by the Cambridge High Performance Computing Service. A.D.F. acknowledges funding from the Science and Technology Facilities Council (STFC), UK, Fellowship No. PP/E0065151.

[1] J. S. Loveday and R. J. Nelmes, High Press. Res. **24**, 45 (2004).
[2] I. Olovsson and D. Templeton, Acta Cryst. **12**, 827 (1959).
[3] J. S. Loveday and R. J. Nelmes, in Science and Technology of High Pressure: Proceedings of AIRAPT-17, edited by M. H. Manghnani, W. J. Nellis, and M. T. Nicol (Universities Press, Hyderabad, India, 2000), pp. 133–136.
[4] J. S. Loveday and R. J. Nelmes, Phys. Rev. Lett. **83**, 4329 (1999).
[5] C. J. Pickard and R. J. Needs, J. Phys.: Condens. Matter **23**, 053201 (2011).
[6] C. J. Pickard and R. J. Needs, Phys. Rev. Lett. **97**, 045504 (2006).
[7] A. D. Fortes, E. Suard, M. H. Lemée-Cailleau, C. J. Pickard, and R. J. Needs, J. Am. Chem. Soc. **131**, 13508 (2009).
[8] A. D. Fortes, E. Suard, M. H. Lemée-Cailleau, C. J. Pickard, and R. J. Needs, J. Chem. Phys. **131**, 154503 (2009).
[9] G. I. G. Griffiths, A. D. Fortes, C. J. Pickard, and R. J. Needs, J. Chem. Phys. **136**, 174512 (2012).
[10] C. W. Wilson, C. L. Bull, G. Stinton, and J. S. Loveday, J. Chem. Phys. **136**, 094506 (2012).
[11] J. Kargel, Icarus **100**, 556 (1992).
[12] A. D. Fortes and M. Choukroun, Space Sci. Rev. **153**, 185 (2010).
[13] A. D. Fortes, I. G. Wood, L. Vočadlo, K. S. Knight, W. G. Marshall, M. G. Tucker, and F. Fernandez-Alonso, J. Appl. Cryst. **42**, 846 (2009).
[14] A. D. Fortes, I. G. Wood, M. Alfredsson, L. Vočadlo, K. S. Knight, W. G. Marshall, M. G. Tucker, and F. Fernandez-Alonso, High Press. Res. **27**, 201 (2007).
[15] A. D. Fortes, Planet. Space Sci. **60**, 10 (2012).
[16] J. Lunine and D. Stevenson, Icarus **70**, 61 (1987).
[17] R. Fu, R. O'Connell, and D. Sasselov, Astrophys. J. **708**, 1326 (2010).
[18] W. Hubbard and J. MacFarlane, J. Geophys. Res. **85**, 225, doi:10.1029/JB085iB01p00225 (1980).
[19] C. Cavazzoni, G. Chiarotti, S. Scandolo, E. Tosatti, M. Bernasconi, and M. Parrinello, Science **283**, 44 (1999).
[20] J. P. Perdew, K. Burke, and M. Ernzerhof, Phys. Rev. Lett. **77**, 3865 (1996).
[21] A. D. Fortes, J. P. Brodholt, I. G. Wood, L. Vočadlo, and H. D. B. Jenkins, J. Chem. Phys. **115**, 7006 (2001).
[22] A. D. Fortes, Ph.D. dissertation, University of London, 2004.
[23] C. J. Pickard and R. J. Needs, Nature Mater. **7**, 775 (2008).
[24] S. Grimme, J. Comput. Chem. **27**, 1787 (2006).
[25] S. J. Clark, M. D. Segall, C. J. Pickard, P. J. Hasnip, M. I. J. Probert, K. Refson, and M. C. Payne, Z. Kristallogr. **220**, 567 (2005).
[26] D. Vanderbilt, Phys. Rev. B **41**, 7892 (1990).
[27] See http://opium.sourceforge.net/ for OPIUM, Pseudopotential Generation Project.
[28] C. Adamo and V. Barone, J. Chem. Phys. **110**, 6158 (1999).
[29] H. J. Monkhorst and J. D. Pack, Phys. Rev. B **13**, 5188 (1976).
[30] S. F. Boys and F. Bernardi, Mol. Phys. **19**, 553 (1970).
[31] A. J. Sadlej, Theor. Chim. Acta **79**, 123 (1991).
[32] R. Bukowski, J. Sadlej, B. Jeziorski, P. Jankowski, K. Szalewicz, S. A. Kucharski, H. L. Williams, and B. M. Rice, J. Chem. Phys. **110**, 3785 (1999).
[33] H. L. Williams, E. M. Mas, K. Szalewicz, and B. Jeziorski, J. Chem. Phys. **103**, 7374 (1995).
[34] T. Helgaker, H. J. A. Jensen, P. Joergensen, J. Olsen, K. Ruud, H. Aagren, A. Auer, K. Bak, V. Bakken, O. Christiansen, S. Coriani, P. Dahle, E. K. Dalskov, T. Enevoldsen, B. Fernandez, C. Haettig, K. Hald, A. Halkier, H. Heiberg, H. Hettema, D. Jonsson, S. Kirpekar, R. Kobayashi, H. Koch, K. V. Mikkelsen, P. Norman, M. J. Packer, T. B. Pedersen, T. A. Ruden, A. Sanchez, T. Saue, S. P. A. Sauer, B. Schimmelpfennig, K. O. Sylvester-Hvid, P. R. Taylor, and O. Vahtras, DALTON, a molecular electronic structure program, release 2.0, 2005; see http://www.kjemi.uio.no/software/dalton/dalton.html.
[35] A. J. Misquitta and A. J. Stone, CamCASP, a program for studying intermolecular interactions and for the calculation of molecular properties in distributed form, University of Cambridge, 2007; see http://www-stone.ch.cam.ac.uk/programs.html#CamCASP.
[36] A. J. Misquitta and K. Szalewicz, Chem. Phys. Lett. **357**, 301 (2002).
[37] A. J. Misquitta, B. Jeziorski, and K. Szalewicz, Phys. Rev. Lett. **91**, 33201 (2003).
[38] A. J. Misquitta, R. Podeszwa, B. Jeziorski, and K. Szalewicz, J. Chem. Phys. **123**, 214103 (2005).
[39] A. J. Cohen, P. Mori-Sánchez, and W. Yang, Science **321**, 792 (2008).
[40] F. Birch, Phys. Rev. **71**, 809 (1947).
[41] A. J. Morris and C. J. Pickard, LINDOS – Version 1.3 User Manual, University College London, 2011.
[42] A. D. Fortes, Institut Laue-Langevin Experimental Report Nos. 5-24-423, 2011; 5-24-469, 2012.
[43] J. S. Loveday, R. J. Nelmes, C. L. Bull, H. E. Maynard-Casely, and M. Guthrie, High Press. Res. **29**, 396 (2009).
[44] C. Ma, F. Li, Q. Zhou, F. Huang, J. Wang, M. Zhang, Z. Wang, and Q. Cui, RSC Adv. **2**, 4920 (2012).
[45] See supplementary material at http://dx.doi.org/10.1063/1.4737887 for further details of the *ab initio* random structure searching.